Electronic Supplementary Material (ESI) for Journal of Materials Chemistry A.

Supporting Information

Functional Group Substitution Strongly Influences the Performances of Covalent Organic Frameworks in the Photocatalytic Metal-Free Oxidase Reaction

Huiying Chen, Qinghai Zhou, Jinyang Hai, Mingxiang Zhu*, Fang Zhang*

Department of Chemistry, Shanghai Normal University 100 Guilin Rd., Shanghai, 200234, China

Corresponding authors:

* Mingxiang Zhu (E-mail: mingxiangzhu@shnu.edu.cn)

* Fang Zhang (E-mail: zhangfang@shnu.edu.cn)

1. Experimental Section

1.1 Chemicals. 4,4',4"- (1,3,5-triazine-2,4,6-triyl) trianiline (TTA), 1,3,5-Tris(4-aminophenyl)benzene (TAPB), 2,5-dimethoxy-1,4-benzenedicarboxaldehyde, 2,5-dibromo-1,4-benzenedicarbox-aldehyde and 2,5-dichloroterephthalaldehydewere supplied by Shanghai Tengqian Biotechnology Co., Ltd. 2,5-dihydroxy-1,4-benzenedicarboxaldehyde, Jilin Chinese Academy of Sciences - Yanshen Technology Co., Ltd (Jilin, China). 1,4-benzenedicarboxaldehyde was purchased from TCI AMERICA. 1,4-Dioxane was purchased from J&K Scientific. Mesitylene and solvents were purchased from Aladdin Company. The reagents were directly used for the experiments without any further purification.

1.2 Mannich reaction process of tetrahydroisoquinolines with acetone.

In a typical experiment, tetrahydroisoquinoline derivatives (0.2 mmol), acetone (2.0 mmol), L- proline (0.06 mmol), COF (4.0 mg) and methanol (2.0 mL) were mixed in were added in a quartz vial with magnetic stirring bar. Subsequently, the mixture was sonicated and stirred for 20 minutes. After that, the mixture was bubbled with an oxygen stream for 5 minutes and an oxygen ball was added. Then, it was irradiated using a 30 W blue LED lamp under rapid stirring for 1.0 h at 25 °C. Thin layer chromatography (TLC) is used to monitor the progress of the reaction. After the reaction, the solvent was removed in vacuum, and the crude product was purified by column chromatography, and the separation yield was calculated.

1.3 Calculation method for catalytic tests.

The conversion and yield were determined by HPLC analysis with internal standard of naphthalene. The detailed description is as follows.

$$\text{Conversion } (\mathbf{1a}) = \left(1 - \frac{A(\mathbf{1a}),r}{A(internal\ Standard),r}\right) / \left(\frac{A(\mathbf{1a}),s}{A(internal\ Standard),s}\right)$$

1a:2-phenyl-1,2,3,4-tetrahydroisoquinoline. A(**1a**), r and A(internal standard), r are the peak areas of the corresponding compounds in the HPLC of the after reaction, A(**1a**),s and A(internal standard),s are the peak areas of the corresponding compounds in the HPLC of the standard samples.

The yield of product Yield (**3a**) was determined by applying the following equations:

$$\text{Yield (3a)} = \left(\frac{A(3a),r}{A(internal\ Standard),r} \Big/ \frac{A(3a),s}{A(internal\ Standard),s}\right)*100\%$$

3a:1-(nitromethyl)-2-phenyl-1,2,3,4-tetrahydroisoquinoline. A(**3a**),r and A(internal standard),r are the peak areas of the corresponding compounds in the HPLC of the after reaction, A(**3a**),s and A(internal standard),s are the peak areas of the corresponding compounds in the HPLC of the standard samples.

1.4 Characterization. PXRD data were obtained using a Rigaku D/Max-B with Cu Kα radiation source. The scanning range is 2-30°, and the scanning speed is 2°/min. The morphology was determined by field emission scanning electron microscopy (FESEM, HITACHI, S-4800). Fourier transform infrared (FT-IR) spectra were recorded using a Nicolet Magna 550 spectrometer. Nitrogen adsorption–desorption isotherms were tested at 77 K by using a TriStar II 3020 V1.03 analyzer. All samples were degassed at 120°C for 10 h. UV-Vis diffuse reflectance spectra were collected on a UV-Vis spectrophotometer (UV-Vis diffuse reflectance spectrometer, were performed using an electrochemical analyzer (CHI 760e Instruments) in a standard three-electrode system.The $\bullet O_2^-$ radicals was monitored by electron paramagnetic resonance spectrometer (EPR, Bruker, EMX-8/2.7).

1.5 The calculation of the band gap of COFs.

The Kubelka-Munk equation is used to determine the band gap energy.

$$(\alpha h\nu)^n = A(h\nu - E_g)$$

Where α represents the absorption coefficient, h is Planck constant, ν is optical frequency, A is the constant, and n is related to the semiconductor type. The value of

direct bandgap semiconductor n is 1/2, and that of indirect bandgap semiconductor n is 2.[1]

1.6 The calculation of valence band/conduction band of COFs.

The Mott-Schottky equation was used to compute the flat band potential (E_{FB}):

$$\frac{1}{C^2}=\frac{2}{Ne\varepsilon_r\varepsilon_0}(E-E_{FB}-\frac{kT}{e})$$

where E is the applied potential, E_{FB} is the flat band potential, T is the temperature, k is the Boltzmann constant, N is the electron carrier density, e is the elemental charge, ε_0 is the permittivity of a vacuum, $\varepsilon_r$is the relative permittivity of the semiconductor, and C is the space charge capacitance.[2] According to the Nernst equation,

$$E_{FB}\ (NHE) = E_{FB}\ (Ag/AgCl) + 0.197$$

Because the position of conductor band (CB) in n-type semiconductors is more negative by about 0.2 V than the flat band potential,[3] so

$$E_{CB}\ (NHE)= E_{FB}\ (NHE)-0.2$$

$$E_{VB} = E_{CB}+ E_g$$

2. Results and Discussion

2.1. Characterization

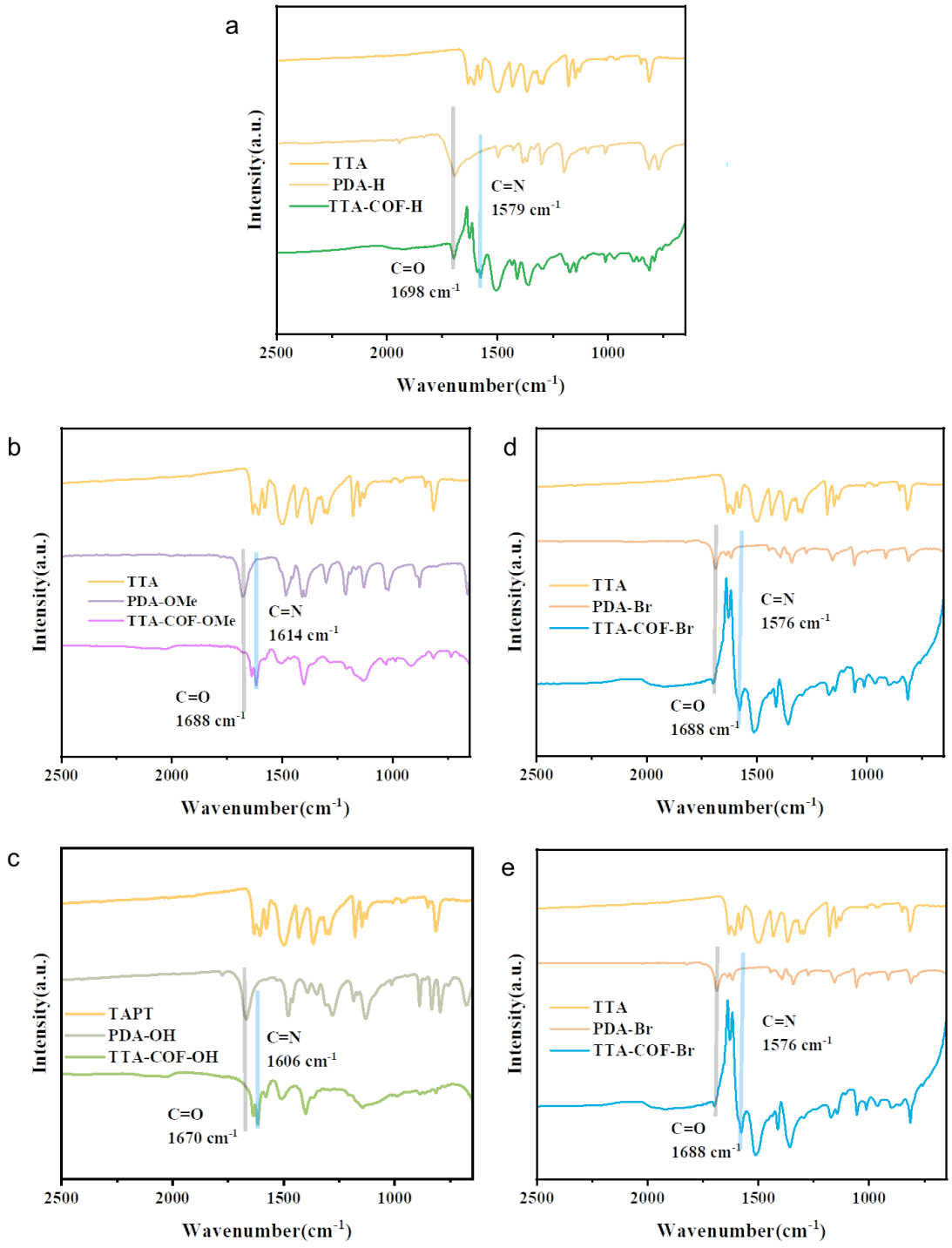

Fig. S1. FTIR spectra of TTA-COF-H(a), TTA-COF-OMe(b), TTA-COF-OH(c), TTA-COF-Br(d) and TTA-COF-Cl(e).

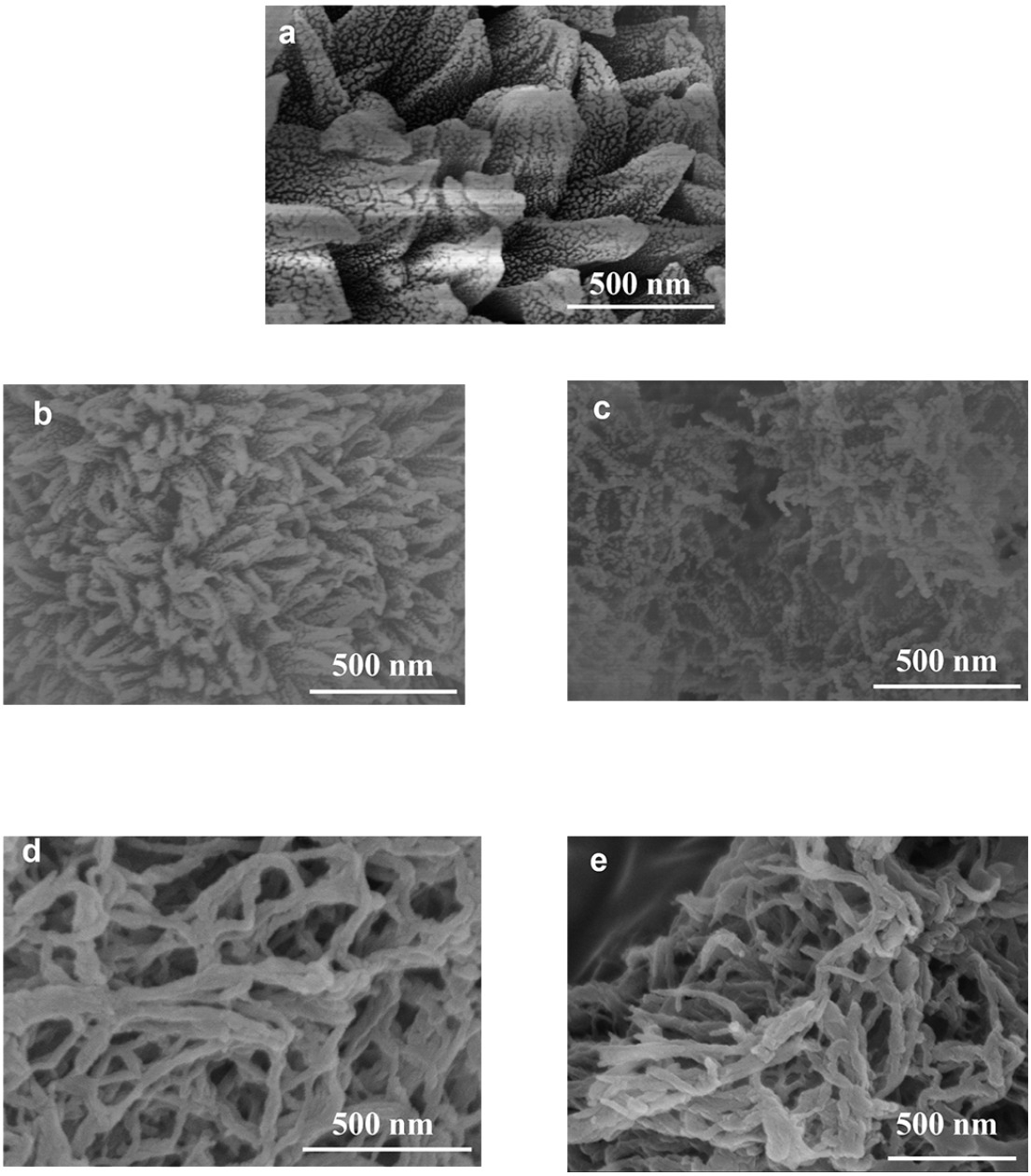

Fig. S2. FESEM image of TTA-COF-H(a), TTA-COF-OMe(b), TTA-COF-OH(c), TTA-COF-Br(d) and TTA-COF-Cl(e).

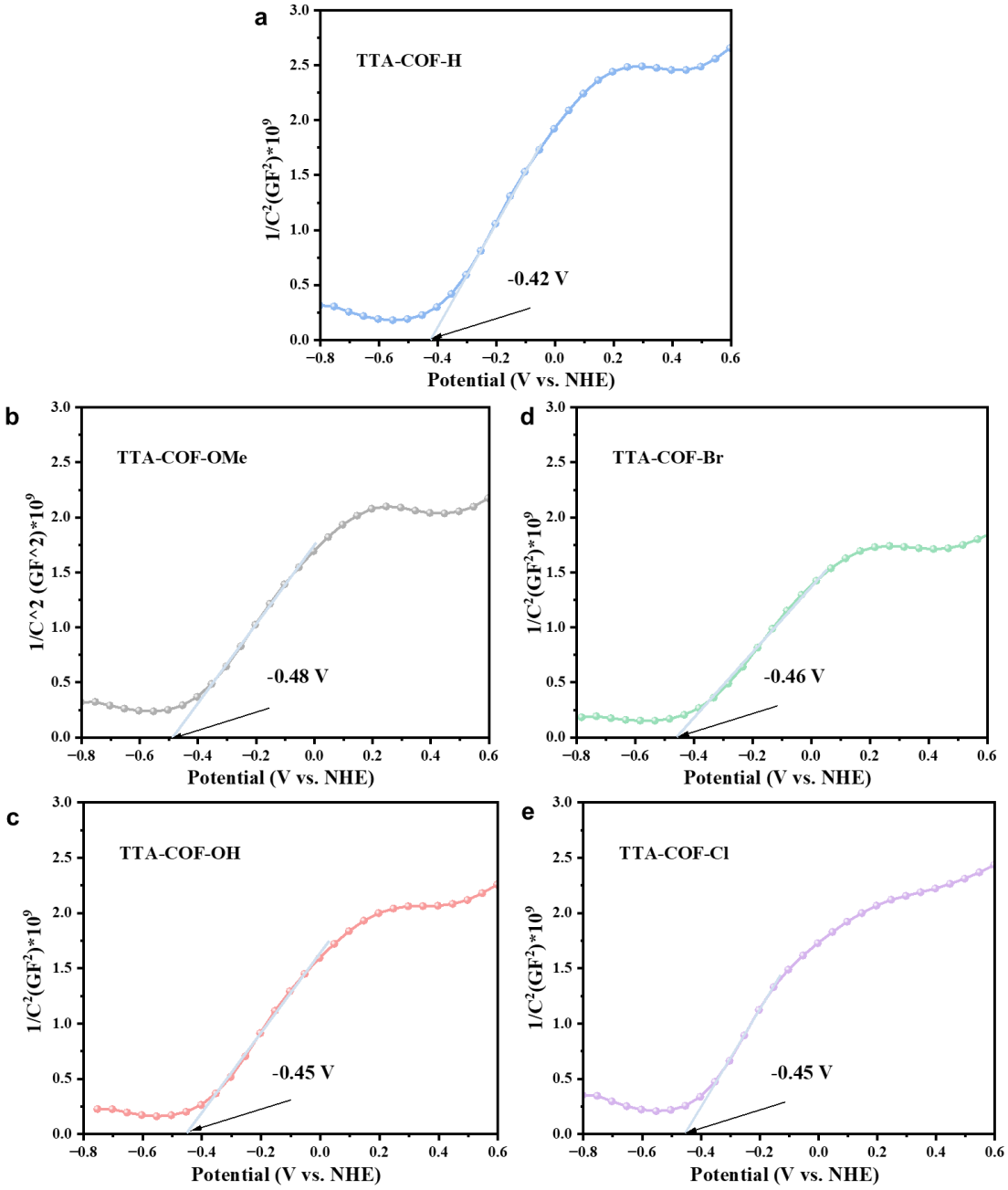

Fig. S3. Mott–Schottky plots of TTA-COF-H(a), TTA-COF-OMe(b), TTA-COF-OH(c), TTA-COF-Br(d) and TTA-COF-Cl(e).

2.2. Further optimization studies

Table S1. Control experiment.[a]

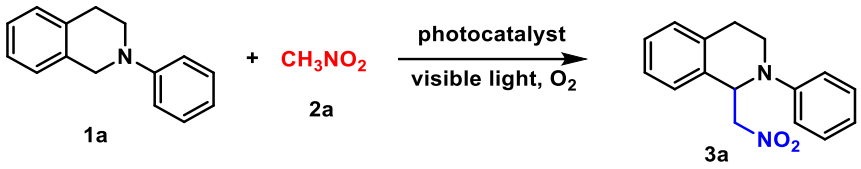

Entry	Conditions	Conversion (%)	Yield (%) [b]
1	standard	84	79
2	blank	<5	trace
3	no photocatalyst	<5	trace
4	N_2	22	20
5	air	39	35

[a]Reaction conditions: **1a** (0.2 mmol), **2a** (0.6 mmol), TTA-COF-Br (4 mg), Methanol (2.0 mL), 25°C, O_2 balloon, Blue LED, 1 h; [b]Determined by HPLC analysis with internal standard.

Table S2. Catalytic performances of TTA-COF-Br with different solvents.[a]

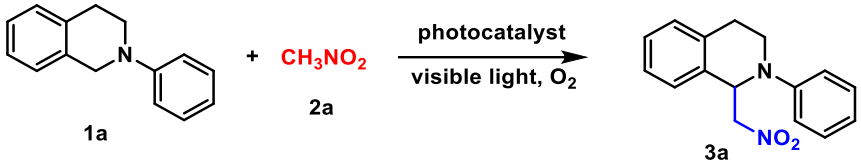

Entry	Solvent	Conversion (%)	Yield (%) [b]
1	Methanol	84	79
2	Ethanol	88	61
3	Acetonitrile	85	48
4	Acetone	98	21
5	Toluene	36	14
6	Cyclohexane	45	26
7	2,2,2-Trifluoroethanol	49	36
8	Hexafluoroisopropanol	30	6

[a]Reaction conditions: **1a** (0.2 mmol), **2a** (0.6 mmol), TTA-COF-Br (4 mg), Solvent (2.0 mL), 25°C, O_2 balloon, Blue LED, 1 h; [b]Determined by HPLC analysis with internal standard.

Table S3. Catalytic performances of varying amounts of TTA-COF-Br. [a]

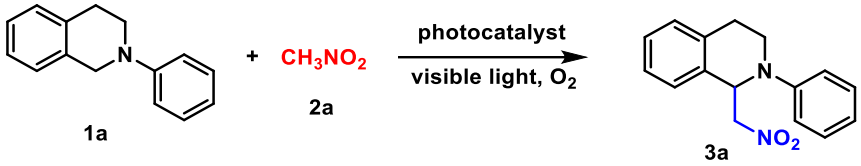

Entry	Catalyst dosage (mg)	Conversion (%)	Yield (%) [b]
1	2	83	16
2	4	84	79
3	6	90	62
4	8	90	60
5	10	91	61

[a]Reaction conditions: **1a** (0.2 mmol), **2a** (0.6 mmol), TTA-COF-Br (x mg), Methanol (2.0 mL), 25°C, O_2 balloon, Blue LED, 1 h; [b]Determined by HPLC analysis with internal standard.

Table S4. Catalytic performances of TTA-COF-Br with different amounts of CH_3NO_2.[a]

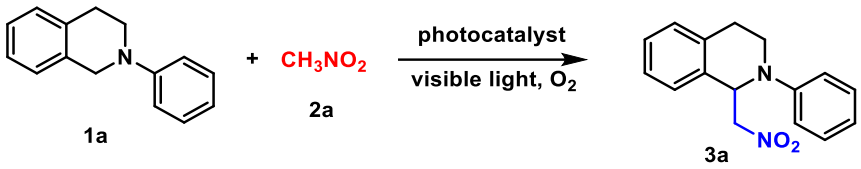

Entry	CH_3NO_2/eq.	Conversion (%)	Yield (%) [b]
1	1	90	36
2	2	88	46
3	3	84	79
4	4	84	61

[a]Reaction conditions: **1a** (0.2 mmol), **2a** (x eqv.), TTA-COF-Br (4 mg), Methanol (2.0 mL), 25°C, O_2 balloon, Blue LED, 1 h; [b]Determined by HPLC analysis with internal standard.

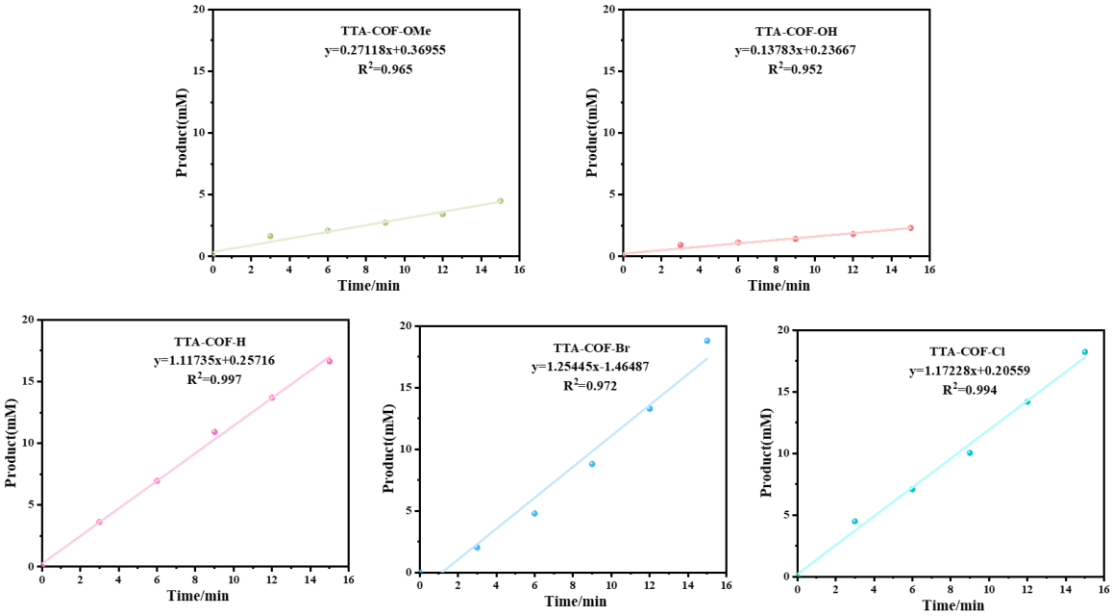

Fig. S4. Plots of **3a** vs. time from initial rate measurement for TTA-COF-R.

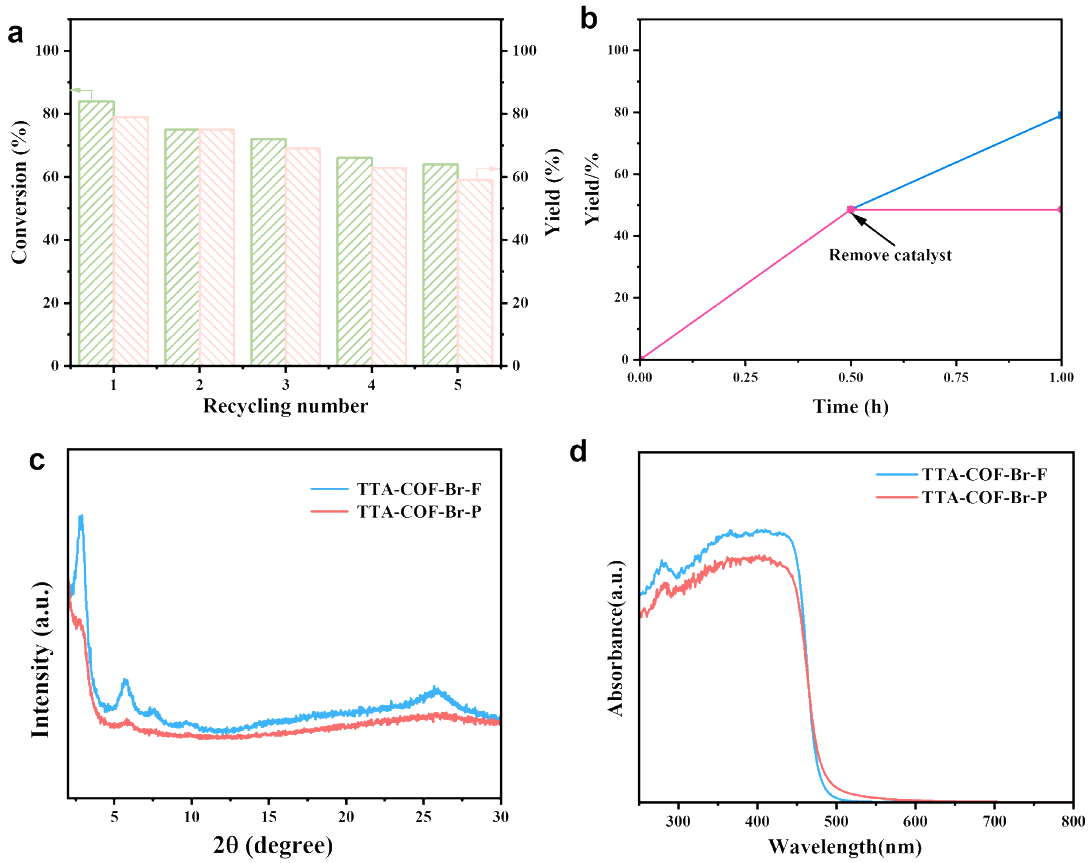

Fig. S5. (a) The reusability of TTA-COF-Br for Aza-Henry reaction of N-phenyl-1,2,3,4-tetrahydroisoquinoline with nitromethane at 25°C for 1 h. (b) Reaction time vs yield (%) curve for the Aza-Henry reaction at 25°C (blue line), after removing the COF at ~50% product formation. (c) PXRD curves of TTA-COF-Br before (blue line) and after the fifth run (red line). (d) UV-Vis spectra of TTA-COF-Br before (blue line) and after the fifth run (red line).

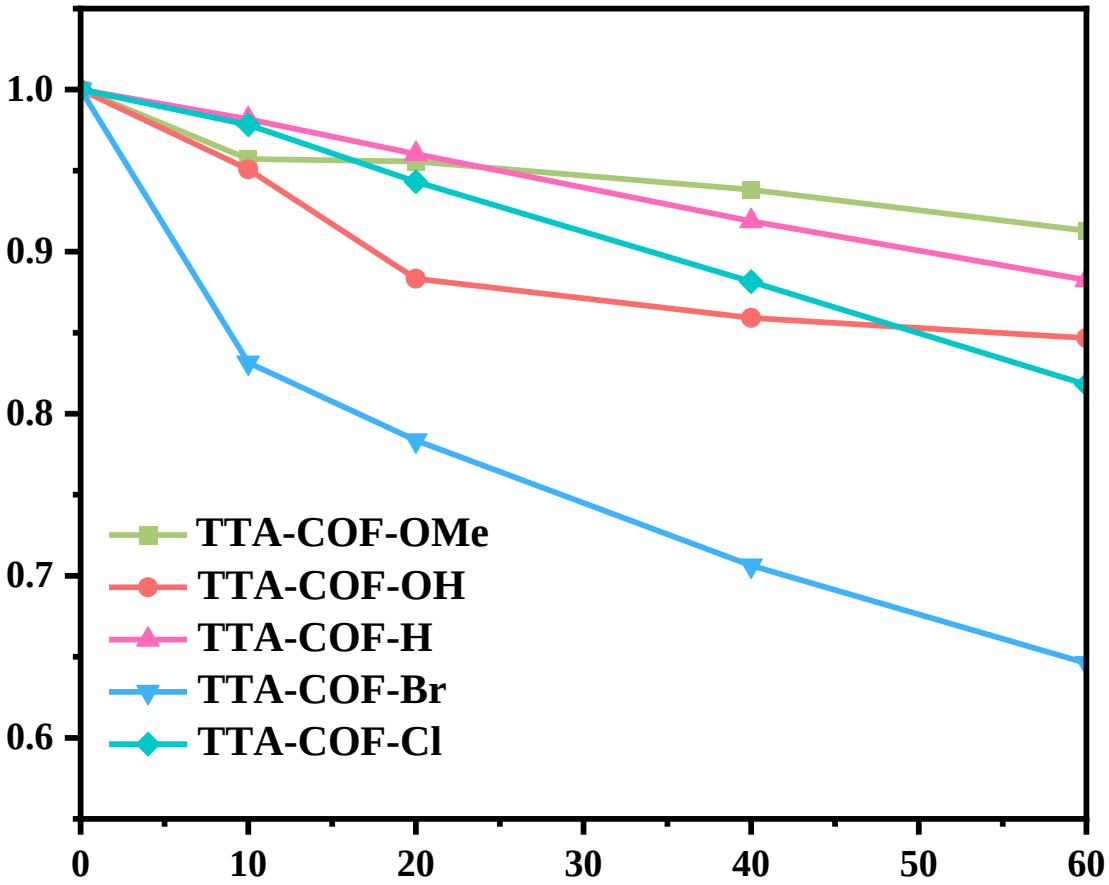

Fig. S6. Consumption of NBT in the visible-light-driven photocatalytic system catalyzed by the COFs.

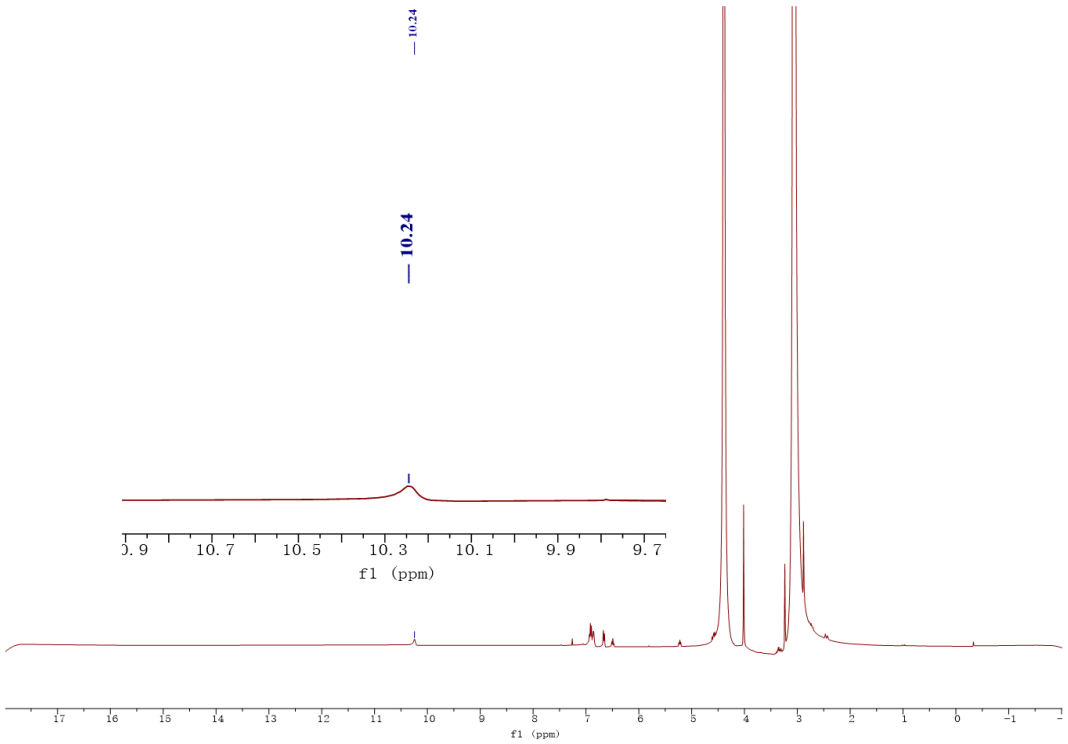

Fig. S7. ^{1}H NMR determination of the H_2O_2 generated in the photocatalytic reactions. The peak at 10.24 ppm is due to H_2O_2 ($CDCl_3$, 400 MHz)

Table S5. Absolute electronic and Gibbs free energy for PC-n(n=1,2,3,4,5) in ground state (S0) and vertical/adiabatic electronic state. Calculated at B3LYP/6-31G(d,p) level in gas phase.

Entry	S0		(VEA[1])	AEA[1]	
	Electronic energy (Hartree)	Gibbs free energy (Hartree)	Electronic energy (Hartree)	Electronic energy (Hartree)	Gibbs free energy (Hartree)
	Charge: 0; Multiplicity: 1		Charge: -1; Multiplicity: 2		
PC-1	-458.89544033	-458.80972900	-458.92326459	-458.93194526	-458.84880900
PC-2	-609.35659391	-609.26204600	-609.39567665	-609.40554681	-609.31378000
PC-3	-687.94131899	-687.79666200	-687.96480362	-687.97409982	-687.83205700
PC-4	-484.42489209	-484.36660900	-484.47821890	-484.48807505	-484.43215600
PC-5	-1378.06620846	-1378.00411100	-1378.11470060	-1378.12419829	-1378.06417700

Note: [1.] VEA stands for “vertical electronic affinity” and AE for “adiabatic electronic affinity”.

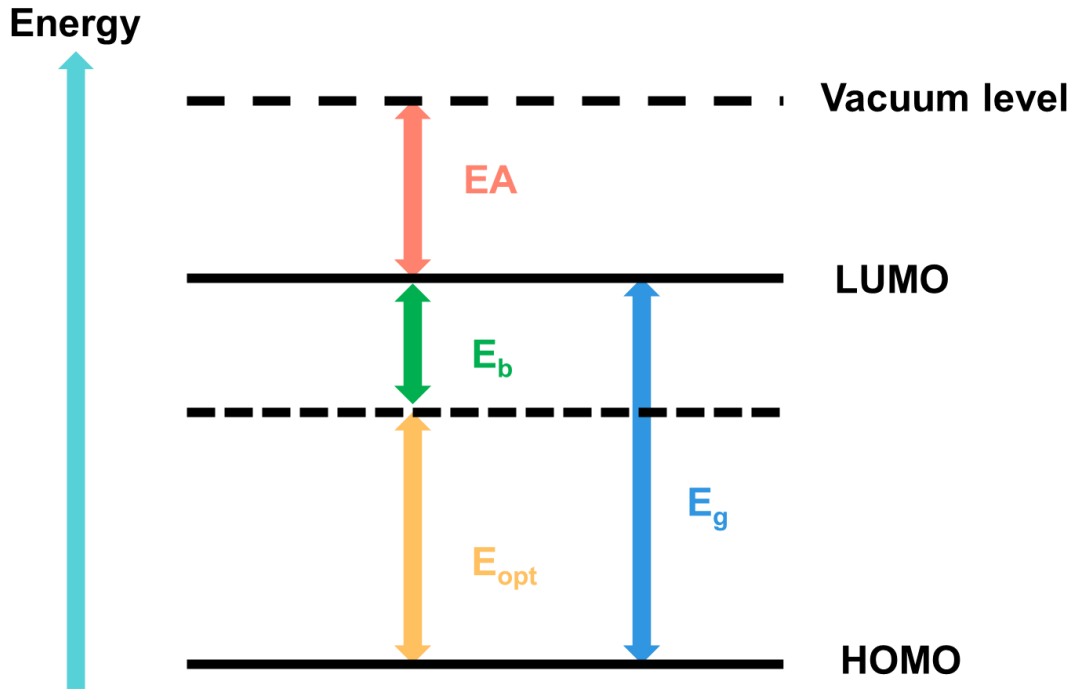

Fig. S8. Illustration of various energy gaps in the molecular base: EA: electron affinity; E_g: HOMO-LUMO gap; E_{opt}: optical gap; E_b: exciton binding energy.

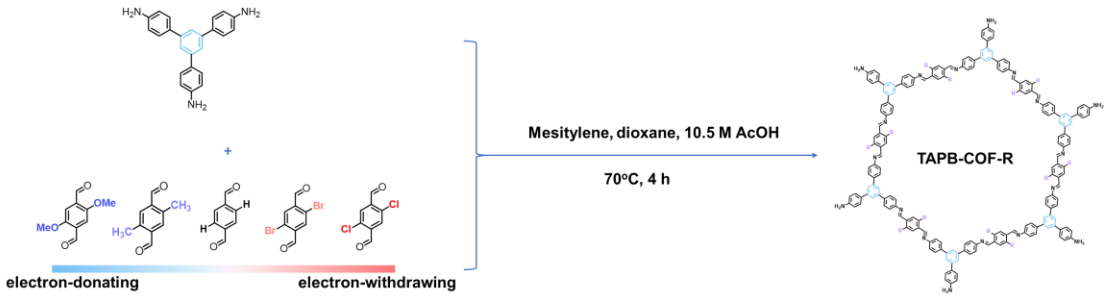

Fig. S9. Schematic illustration of the synthesis of TAPB-COF-R.

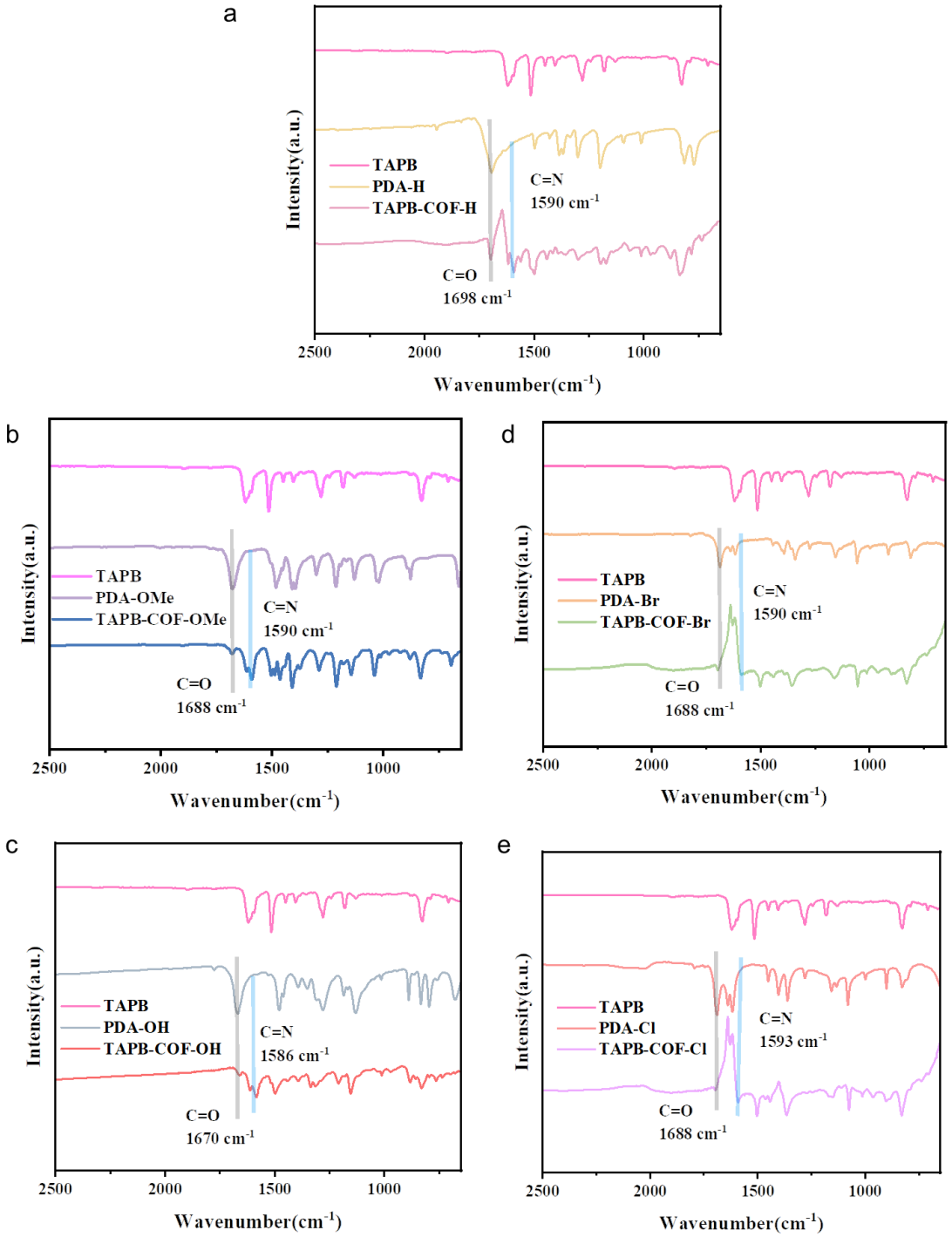

Fig. S10. FTIR spectra of TAPB-COF-H(a), TAPB-COF-OMe(b), TAPB-COF-OH(c), TAPB-COF-Br(d) and TAPB-COF-Cl(e).

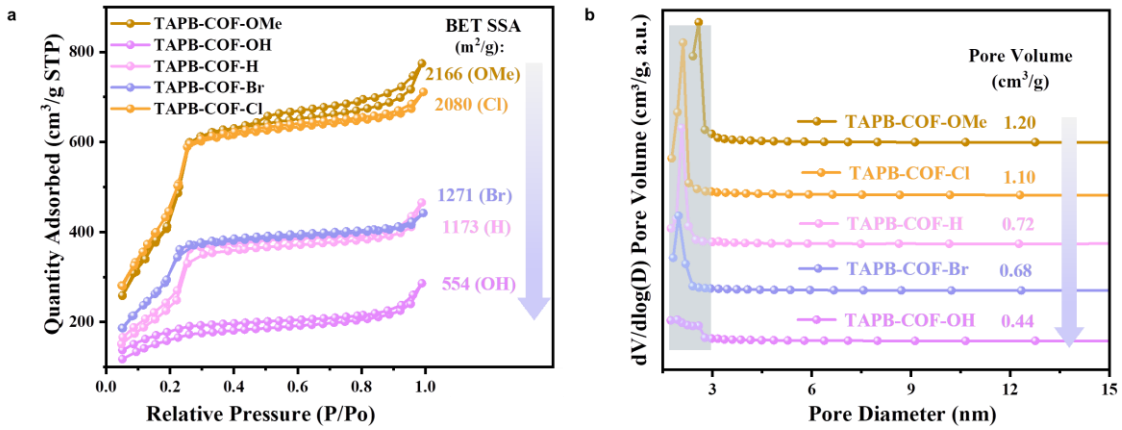

Fig. S11. (a) Nitrogen-sorption isotherms measured at 77 K and (b) Pore size distribution profiles of TAPB-COF-R.

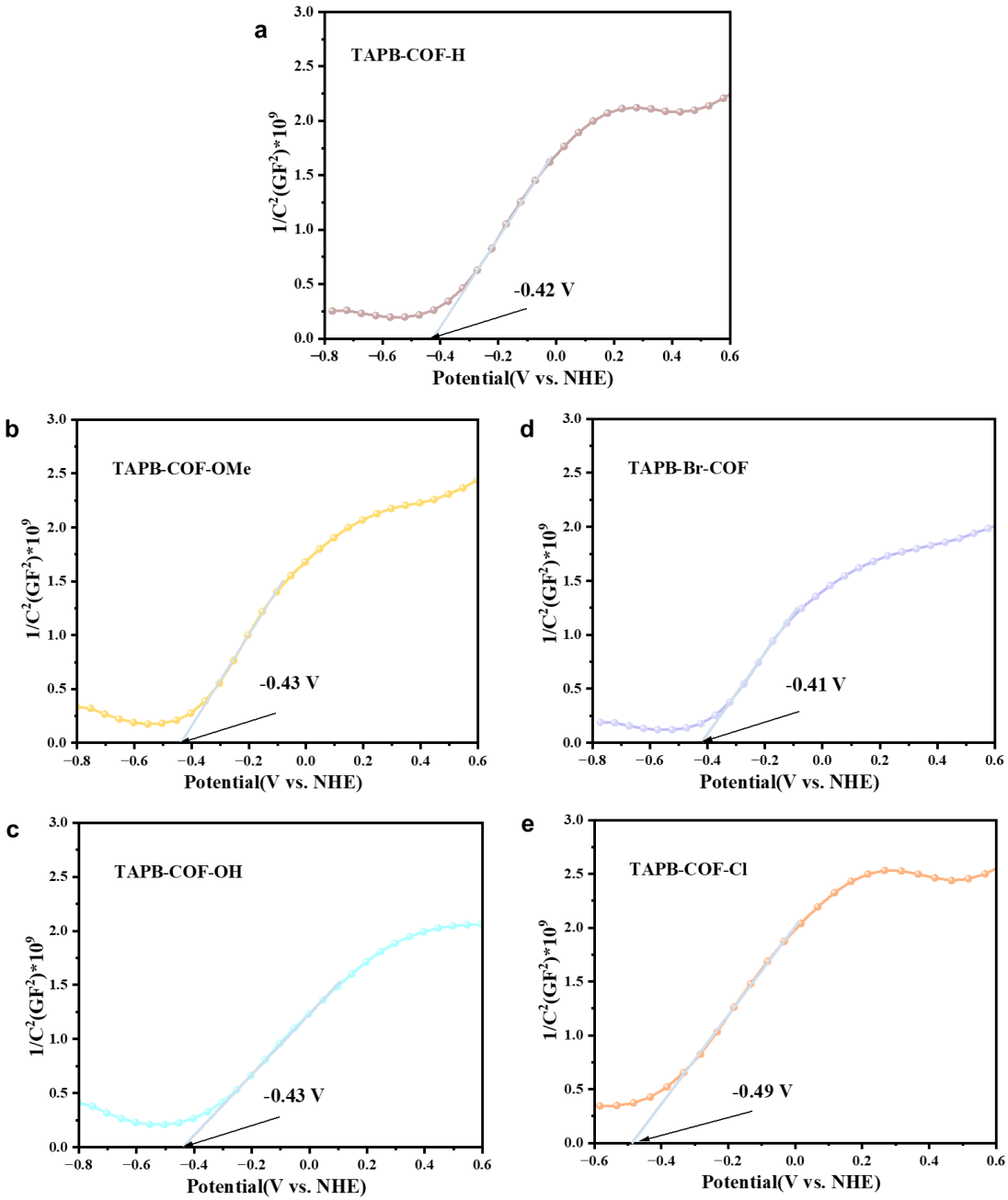

Fig. S12. Mott–Schottky plots of TAPB-COF-H(a), TAPB -COF-OMe(b), TAPB -COF-OH(c), TAPB -COF-Br(d) and TAPB -COF-Cl(e).

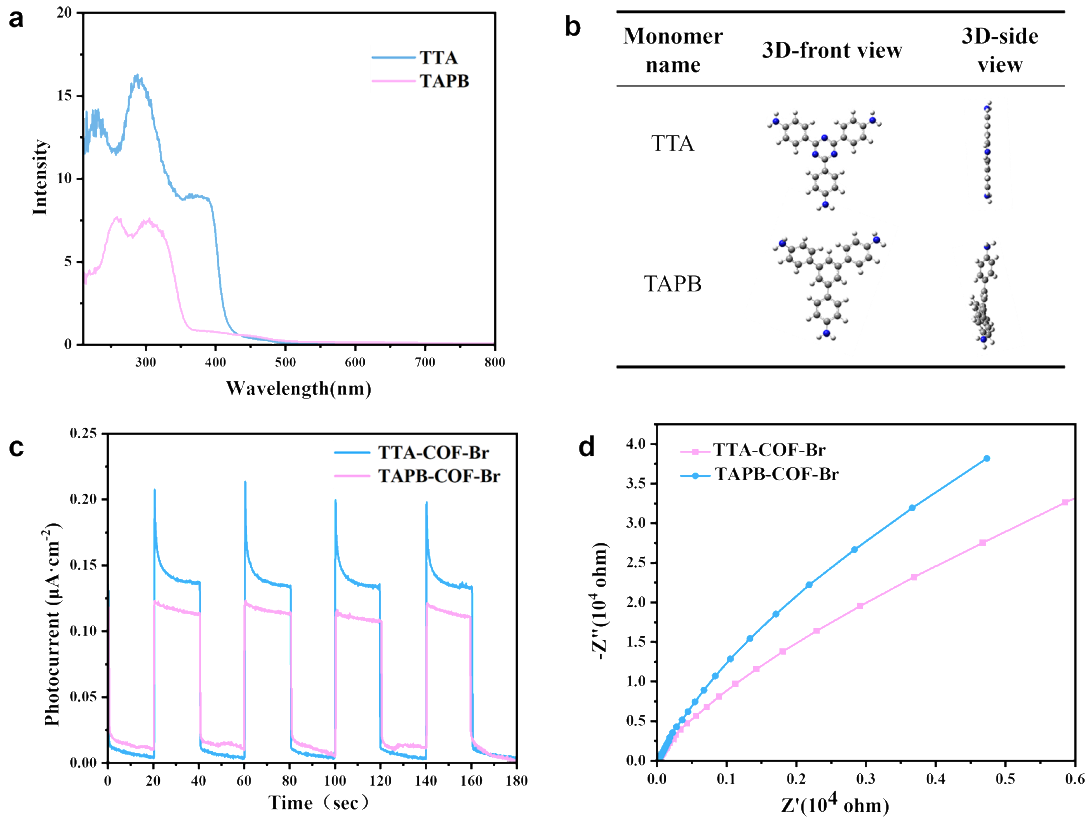

Fig. S13. (a) UV-DRS of TTA and TAPB. (b) DFT geometry optimization of TTA and TAPB. (c) Transient photocurrent responses of TTA-COF-Br and TAPB-COF-Br. (d) Electrochemical impedance spectroscopy of TTA-COF-Br and TAPB-COF-Br.

References

1 H. Wang, R. Zhao, H. Hu, X. Fan, D. Zhang and D. Wang, *ACS Appl. Mater. Interfaces*, 2020, **12**, 40176-40185.

2 X. Chen, Y. Cai, R. Liang, Y. Tao, W. Wang, J. Zhao, X. Chen, H. Li and D. Zhang, *Appl. Catal. B Environ.* 2020, **267**, 118687.

3 Z. Xu, J. Hu, H. Dong, Y. Zhu and M. Zhu, *J. Colloid Interface Sci.*, 2022, **626**, 599-607.